13.2

INVITED

EXPERIMENTS IN MAGNETIC SWITCHING

D. L. Birx, E. J. Lauer, L. L. Reginato, D. Rogers Jr., M. W. Smith, T. Zimmerman
University of California, Lawrence Livermore National Laboratory, Livermore, CA 94550

Abstract

Magnetic switching offers an alternative to overcoming the rep-rate and life limitations of the spark gaps in the ETA/ATA induction accelerators. The principle has been applied for many years to radar modulators but at much lower power levels and longer pulse lengths. Comparatively recent developments in magnetic materials together with some optimal circuits have made it possible to go well beyond the state of the art. A magnetic modulator has been built which steps up and compresses a 25 kV, 5 μs pulse into a 250 kV, 50 ns pulse. A second magnetic modulator has been built and installed to replace four Blumleins and spark gaps in order to provide triggers for the complete ETA injector and accelerator. The paper outlines some practical and theoretical considerations affecting the design of the magnetic pulse generator.

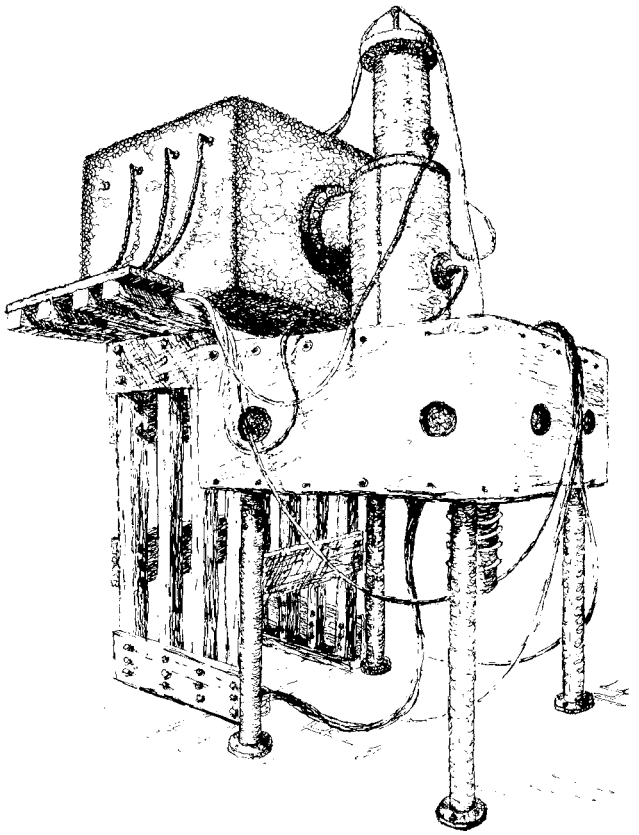

Introduction

The limitations of life and rep-rates expected from high pressure gas blown switches have led us to re-examine the technique of pulse time compression by using saturable reactors. This technique was first described by Melville[1] in 1951 and has been used in the past and in recent years to generate high power (10^5 W) pulses for radar. There was little doubt that this technology could be used to produce very high power levels ($> 10^{10}$ W) and very high rep-rates (> 1 kHz). Although magnetic switches have not been built to operate at this power level, we were confident that it was achievable by applying proper high voltage techniques. As far as repetition rates, it was clear that there would be no limitations except those imposed by the charge time of the first stage and the time to reset all the cores. The more challenging problem, therefore, consisted in generating the 50-70 ns pulse with reasonable rise time and efficiency. Comparatively recent developments in magnetic materials with high ΔB and very low eddy current losses have made it possible to achieve the desired parameters.

Operation

The theory of operation of magnetic modulators and the conditions for optimum operation have been described in several reports.[1-7] It is briefly repeated here for continuity.

The basic principle behind magnetic switching is to use the large changes in permeabilities exhibited by saturating ferri- (ferro-) magnetic material to produce large changes in impedance. The standard technique for capitalizing on this behavior is illustrated in Fig. 1. By using multiple stages as shown, it is possible to achieve an effective change in impedance much larger than can be obtained from a single stage. The operation of this circuit can be described as follows.

Capacitor C_1 is charged through L_0 until L_1 saturates; L_1 is chosen to have a saturated inductance much less than L_0. Once L_1 saturates, C_2 will begin to charge from C_1 through L_1, but because $L_{1sat} \ll L_0$, C_2 charges much more rapidly than C_1 did. The process continues through the successive stages until C_n discharges into the load. Each successive saturable reactor is designed so that saturation occurs at the peak of the voltage. For optimum energy transfer, each successive capacitor is of equal or slightly smaller value than the preceding one depending on the amount of energy lost in the saturable reactor.

The analysis which follows is based on saturable inductors with toroidal geometries, and for the sake of clarity several simplifying approximations have been introduced. All circuit components will be assumed lossless and all extraneous inductances ignored. Also, the expressions for saturated inductance will assume that the area enclosed by the turns is simply the core cross sectional area, while in practice insulation between turns will result in a larger saturated inductance.

Saturation of an inductor occurs when the magnetic field in the inductor core reaches the saturation magnetization. This assumes of course that the core material is ferri- or ferromagnetic material. Saturation is measurable as a large incremental change in the material permeability. According to Maxwell,

$$\int E \cdot d\ell = V_L = N \frac{\partial \Phi}{\partial t} = NA \frac{\partial B}{\partial t} , \qquad (1)$$

Report Documentation Page

Form Approved
OMB No. 0704-0188

1. REPORT DATE	2. REPORT TYPE	3. DATES COVERED
JUN 1981	**N/A**	**-**

4. TITLE AND SUBTITLE	5a. CONTRACT NUMBER
Experiments In Magnetic Switching	5b. GRANT NUMBER
	5c. PROGRAM ELEMENT NUMBER
6. AUTHOR(S)	5d. PROJECT NUMBER
	5e. TASK NUMBER
	5f. WORK UNIT NUMBER
7. PERFORMING ORGANIZATION NAME(S) AND ADDRESS(ES) **University of California, Lawrence Livermore National Laboratory, Livermore, CA 94550**	8. PERFORMING ORGANIZATION REPORT NUMBER
9. SPONSORING/MONITORING AGENCY NAME(S) AND ADDRESS(ES)	10. SPONSOR/MONITOR'S ACRONYM(S)
	11. SPONSOR/MONITOR'S REPORT NUMBER(S)

12. DISTRIBUTION/AVAILABILITY STATEMENT
Approved for public release, distribution unlimited

13. SUPPLEMENTARY NOTES
See also ADM002371. 2013 IEEE Pulsed Power Conference, Digest of Technical Papers 1976-2013, and Abstracts of the 2013 IEEE International Conference on Plasma Science. Held in San Francisco, CA on 16-21 June 2013. U.S. Government or Federal Purpose Rights License.

14. ABSTRACT
Magnetic switching offers an alternative to overcoming the rep-rate and life limitations of the spark gaps in the ETA/ATA induction accelerators. The principle has been applied for many years to radar modulators but at much lower power levels and longer pulse lengths. Comparatively recent developments in magnetic materials together with some optimal circuits have made it possible to go well beyond the state of the art. A magnetic modulator has been built which steps up and compresses a 25 kV, 5 ~s pulse into a 250 kV, 50 ns pulse. A second magnetic modulator has been built and installed to replace four Blumleins and spark gaps in order to provide triggers for the complete ETA injector and accelerator. The paper outlines some practical and theoretical considerations affecting the design of the magnetic pulse generator.

15. SUBJECT TERMS

16. SECURITY CLASSIFICATION OF:			17. LIMITATION OF ABSTRACT	18. NUMBER OF PAGES	19a. NAME OF RESPONSIBLE PERSON
a. REPORT	b. ABSTRACT	c. THIS PAGE			
unclassified	**unclassified**	**unclassified**	**SAR**	**7**	

$$\int V_L dt = NA\ \Delta B\ , \qquad (2)$$

and if the core has been reset,

$$\int_0^{\tau_{sat}} V_L dt = NA(B_r + B_s) = NA\ \Delta B\ , \qquad (3)$$

where N is the number of turns around the core, A is the area of the core, and $B_r(B_s)$ the remanent (saturating) magnetic field. It may be advantageous in cases wehre B_r is small to use an "active" type of reset to achieve a larger ΔB. That is, choose the timing so that the reset current is still flowing during the main output pulse.

Fig. 1 Magnetic Switch

Fig. 1a Multistage Saturable Reactor

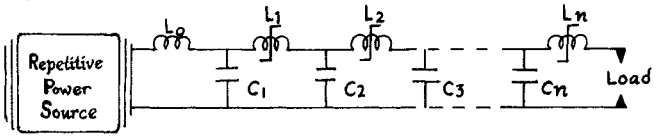

Fig. 1b Waveforms

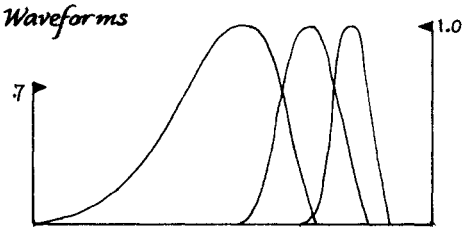

Returning now to Fig. 1a, it can be shown that the time required to charge capacitor C_n after L_{n-1} saturates is given by

$$\tau_{charge}^{C_n} = \tau_{discharge}^{C_{n-1}} = \pi\left(L_{n-1}^{sat} \cdot \frac{C_{n-1}\,C_n}{C_{n-1} + C_n}\right)^{1/2} \qquad (4)$$

but if $C_n = C_0$ | all n, then

$$\tau_{charge}^{C_n} = \pi\left(\frac{L_{n-1}^{sat} \cdot C_0}{2}\right)^{1/2} \qquad (5)$$

The time required to charge capacitor C_n should be approximately equal to the time to reach B_{sat} in inductor L_n. Therefore

$$\tau_{sat}^{L_n} \simeq \tau_{charge}^{C_n} = \frac{\Delta B_s\, N_n\, A_n}{\langle V_c \rangle}\ . \qquad (6)$$

Ideally

$$\langle V_C \rangle = V_{C0} \int_0^{\pi/\omega} \frac{(1 - \cos \omega\tau)}{2}\, dt = \frac{V_{C0}}{2}\ ; \qquad (7)$$

therefore

$$\tau_{charge}^{C_n} = \frac{2\,\Delta B_s}{V_{C0}}\, N_n A_n\ , \qquad (8)$$

where V_{C0} is the peak charge voltage of capacitor C_n. After inductor L_n saturates we find:

$$L_n = \frac{\mu_n^{sat}}{2}\, W_n\, N_n^2\, \ell n\left(\frac{R_{on}}{R_{in}}\right) \simeq \frac{\mu_n^{sat}}{2\pi}\, \frac{N_n^2 A_n}{\langle R \rangle} \qquad (9)$$

$$\simeq \frac{\mu_n^{sat}\, N_n A_n}{\text{volume}}\ , \qquad (10)$$

where W_n is the axial width of the toroid and $R_{on}(R_{in})$ the core outer (inner) radius. Combining Eqs. (5) and (8) we see that

$$L_{n-1}^{sat} = \frac{2}{C_0}\left(\frac{2}{\pi^2}\, \frac{\Delta B_s}{V_c}\, N_n A_n\right)^2 \qquad (11)$$

Introducing Eq. (10) gives:

$$\frac{L_n^{sat}}{L_{n-1}^{sat}} \simeq \frac{\mu_n^{sat}}{\text{volume}_n} \cdot 2\,\frac{\left(\frac{C_0}{2} V_c^2\right)}{4 \cdot \Delta B_s^2} \approx \frac{\text{energy}}{\text{volume}_n}\left(\frac{\mu_n^{sat} \cdot \pi^2}{4 \cdot \pi B_s^2}\right) \qquad (12)$$

therefore

$$\text{volume}_n = \left(\frac{\tau_{charge}^{C_n}}{\tau_{charge}^{C_{n+1}}}\right)^2 \cdot \text{energy}\left(\frac{\mu_n^{sat}\, \pi^2}{4 \cdot (\Delta B_s)^2}\right) \qquad (13)$$

where

$$\frac{\tau_{charge}^{C_n}}{\tau_{charge}^{C_{n+1}}} = \left(\frac{L_n^{sat}}{L_{n+1}^{sat}}\right)^{1/2} = \text{gain}\ . \qquad (14)$$

It can also be shown that if the core materials are identical, optimal efficiency is achieved when all core volumes are equal.[2] It becomes apparent from the above analyses that for satisfactory operation of a multistage circuit the following conditions must be met:

(a). $L_{n-1}^{\text{saturated}} >> L_n^{\text{unsaturated}}$;

(b). $L_{n+1}^{\text{unsaturated}} >> L_n^{\text{unsaturated}}$;

(c). Saturation of inductor L must occur at π/ω on the charging voltage for C_n;

(d). $C_n \simeq C_0$ for all N; and

(e). The saturated impedance of L_n, the final inductor, must be much less than the load impedance.

A criteria of 20 for >> has been recommended,[1] and experimental work here supports that opinion.

Combining conditions (a) and (b) yields

$$\text{(c).}\quad \frac{L_n^{\text{unsaturated}}}{L_n^{sat}} = \frac{\mu_{unsat}}{\mu_{sat}} \geq 400\ .$$

This condition allows us to generate an approximate expression for the maximum practical compression factor per stage:

$$\frac{\tau_{n-1}}{\tau_n} = \left(\frac{L_{n-1}^{unsat}}{L_n^{sat}}\right)^{1/2} \leq \left(\frac{\mu_{unsat}}{\mu_{sat} \cdot 20}\right)^{1/2} \qquad (15)$$

Hence, given the desired overall compression factor, the minimum number of stages can be determined from the material properties.

It should also be noted here that in general the effective unsaturated permeability is a function of the saturation time unless eddy current and spin relaxation losses can be neglected. In addition, the saturated permeability can be a strong function of the applied H field up to several thousand A-T/m and in actuality is never identically equal to μ_0. These topics are addressed in more detail in Appendix A.

Experimental Magnetics Pulse Generator

As a demonstration of the principle, a small scale magnetic pulse generator was designed and constructed. The goal was to compress a 15 kV, 15 μs charging pulse to a rectangular pulse of 60 ns FWHM into a 1.6 Ω load. This system was constructed from available leftover materials and therefore not fully optimized. The first stage of compression used 50-50 Ni Fe and the last two stages used ETA type of ferrite. The PFN for the first two stages were capacitors and the final stage was 1.6 Ω water filled coax. Even under the non-optimum design parameters agreement between theory and experiment was quite good. The design data and the experimental test results are presented in UCID-18831.[3]

With the confidence gained from the performance of the small scale magnetic switch, the logical next step was to build a larger one to satisfy the energy levels of the ETA Blumlein, 250 kV 50 ns FWHM into a 10Ω load. The goal of this experiment was to check the scaling laws at the higher energy levels ($\sim 10^{10}$ ω) and to obtain a rectangular pulse from the final stage.

The final stage was a spare 10Ω ETA water filled Blumlein with 10 nF capacitance. In order to provide a uniform voltage distribution on the Blumlein it is required that

$$\tau_{charge} >> \tau_{output\ pulse} \qquad (16)$$

It is also a desirable condition that the output pulse risetime be much less than the pulse period:

$$\frac{L_{final}}{R_{out}} << \tau_{output\ pulse} \qquad (17)$$

Rewriting Eqs. (16) and (17) in a more quantitative form gives

$$\tau_{charge} \geq G_1 \cdot \tau_{output\ pulse}, \qquad (18)$$

$$\frac{L_{final}}{R_{out}} \leq \frac{\tau_{output\ pulse}}{G_2}, \qquad (19)$$

where G_1 and G_2 are chosen from the requirements on the output pulse dictated by the load.

Combining Eqs. (18) and (19) we obtain

$$\frac{L_{final}}{R_{out}} \leq (G_1 G_2)^{-1} \tau_{charge}, \qquad (20)$$

$$L_{final} \leq \frac{\left(G_1^2 G_2\right)^{-1} \tau_{charge}^2 R_{out}}{\tau_{output\ pulse}}$$

Now applying Eq. (5) gives

$$\frac{L_{final}^{sat}}{L_{final-1}^{sat}} \leq \frac{\pi^2 \frac{C_0}{2} R_{out} \cdot \left(G_1^2 \cdot G_2\right)^{-1}}{\tau_{output\ pulse}}. \qquad (22)$$

$$\frac{1}{2} C_0 V_c^2 = \frac{\tau_{output}}{R_{out}} \left(\frac{V_c}{2}\right)^2, \qquad (23)$$

and Eq. (22) can be rewritten as

$$(Gain)^2 = \frac{L_{final}^{sat}}{L_{final-1}^{sat}} \leq \frac{\pi^2}{4} \left(G_1^2 \cdot G_2\right)^{-1}. \qquad (24)$$

Combining Eq. (24) with Eq. (15) yields

$$\frac{80\ G_1^2 G_2}{2} \leq \frac{\mu_{unsat}}{\mu_{sat}}. \qquad (25)$$

As the pulse energy increases, we can see that the following simple scaling laws apply:

- maximum gain is independent of pulse energy;
- number of stages is independent of pulse energy;
- efficiency is independent of pulse energy; and
- core volume varies linearly with pulse energy.

These relationships provide an indication of the major problem involved in going to larger and larger systems. Magnetic swtiches for large pulse energies will be bulky and heavy. It is also worth noting that multistage switches require multiple capacitive storage units each capable of storing the full pulse energy, and the capacitor volume will also vary linearly with pulse energy.

To reduce the number of cascaded stages, it is desirable to choose the initial stage to have as fast a charge time as practical. In our case it was convenient to use the same switch chassis as the ETA accelerator. Thyratron voltage and di/dt limitation gives us 20 kV with 5 μs charge time. This voltage is stepped up to 250 kV by a non-saturating transformer which uses 1 mil Ni-Fe core leftover from the Astron accelerator. To satisfy condition (16) 200 ns was chosen for the Blumlein charging

time. There exist various choices for the core materials used in the different stages. The first two stages compressed the input pulse from 5 μs to 200 ns and used 1 mil Ni-Fe as the core material. Although metglas could have yielded lower losses especially in the second stage, availability of the Ni-Fe made it the practical choice. For the final stage since a rectangular pulse output is observed, condition (17) must be satisfied. Although Zn Ferrites were investigated for the final stage, it was obvious that magnetic properties of 2605 metglas would be the optimum choice. Metglas about 1 mil in thickness was readily available from Allied Chemical without insulation on the surface. This material was purchased and wound in our shop by using 1/4 mil mylar as turn to turn insulation; this yielded a packing factor of 0.7. The unavailability of kapton as an insulator eliminated the possibility of annealing the toroids after winding to achieve better performance.

Fig.2 Magnetic Switch

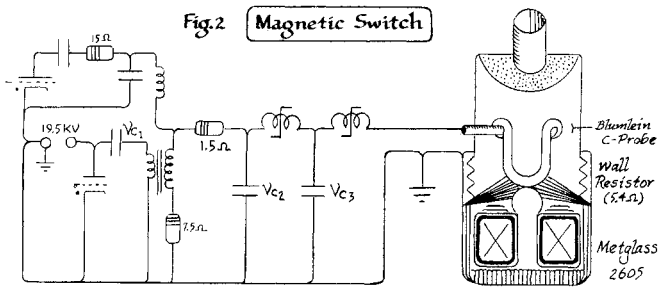

Nevertheless, the magentic modulator, even in the unoptimized design, performed very favorably when compared to the gas blown sparkgap as the discharge device. A summary of the experimental test results are shown in Fig. 3. The rise time achieved was 10 ns and the overall efficiency about 70%. Due to the commitment of this experimental test stand to the low pressure and surface breakdown switches, optimization of the system was not attempted.

Fig.3 Experimental Results

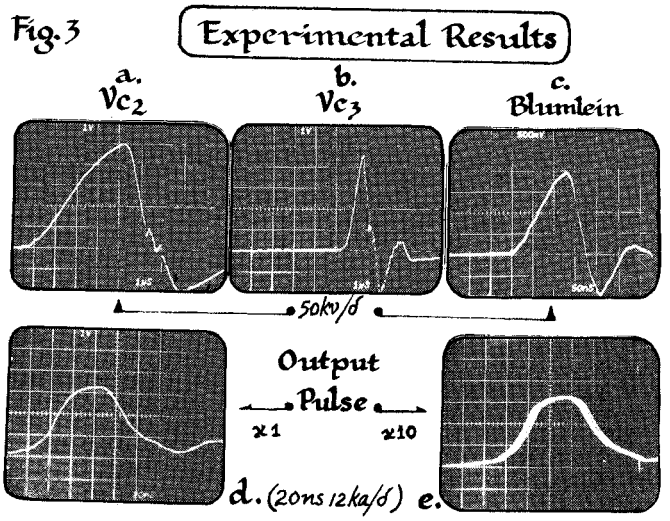

An accelerator such as the ATA would require many parallel pulse generators firing simultaneously to provide the total energy. An area of concern which was further investigated was the discharge time stability. Variations in discharge time would result in jitter between stages which would be unacceptable if it exceeded a few ns. The discharge time is governed by core saturation and proved to be exactly calculable from variations in amplitude of input voltage. Clearly, a well regulated input voltage pulse would yield jitters that are acceptable for the accelerator. Fig. 3e, f shows that the jitter in output pulse is directly related to input pulse amplitude variations.

Magnetic Trigger for ETA Accelerator

Operating experience gained with the two magnetic pulse generators convinced us that they were well suited for applications requiring high reliability and high rep-rates. Although their size and weights are not negligible, their high peak energy capability makes them very effective in driving low impedances or multiple loads. At about this time, the ETA was scheduling a shutdown to replace all the trigger cables and connectors to the sparkgaps. These cables and connectors had proved to be a real limitation to the system and were to be replaced with more reliable ones. Twenty of these cables provide the trigger to the injector and ten go to the accelerator. The triggers are generated from four Blumlein lines switched by gas blown spark gaps. This seemed like an ideal test bed for a magnetic switch. It was decided that the four Blumlein lines with their respective spark gaps would be replaced by a single magnetic pulse generator. The magnetic switch had to be capable of supplying a 120 kV pulse of 50 ns duration into a 2.2Ω load. The design of the ETA trigger generator is very similar to the previously described standard magnetic pulse generator. Pulse flatness was not a requirement but fast rise time was still needed to insure that the gas blown gaps would have low jitter. A block diagram of the new and old ETA trigger systems is shown on Fig. 4. The magnetic pulse generator simplified the system considerably by reducing the quantity and complexity of hardware components. The charging pulse is provided by two simultaneously fired ETA switch chassis which supply a 5 μs 20 kV pulse to the step-up transformer. Four cascaded stages compress the pulse from 5 μs to 100 ns with a risetime of 20 ns. Fig. 5 shows the schematic of the system. The first two stages used slightly larger interstage capacitors to make up for core losses. The only critical aspect of the magnetic switch was the design of the final stage so that condition (17) would be satisfied to obtain a fast risetime in the output pulse. The output stage losses were slightly higher than expected but still provided ample trigger voltage. The ten pulse overlay on Fig. 6f shows that the magnetic modulator indeed provided sufficient voltage for very low jitter in the injector output pulse.

Not considering the reset circuit, the overall efficiency of the magnetic pulse generator is approximately 60%. There is a circuit added to this pulse generator which was not required in the previous one. The ETA trigger system is designed so that near voltage doubling occurs at the trigger electrode as the 68 Ω cables are unterminated (capacitively coupled). Inductor L5 and resistor R5 not only provide a return path for the reset current but provide a terminating impedance for the reflected pulse. L5 is unsaturated for the foward wave but is in the saturated state for the reflected pulse so that the 2.5 Ω resistor provides a matching impedance.

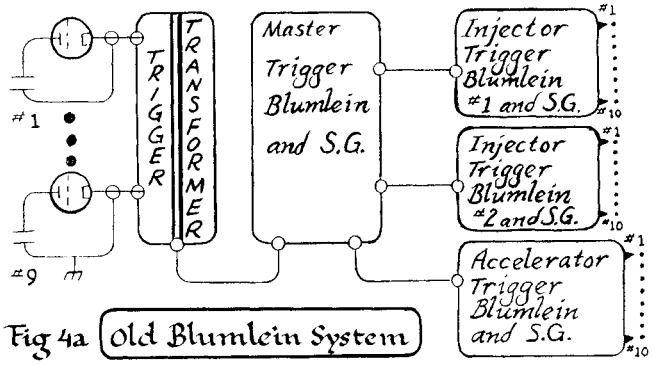

Fig 4a Old Blumlein System

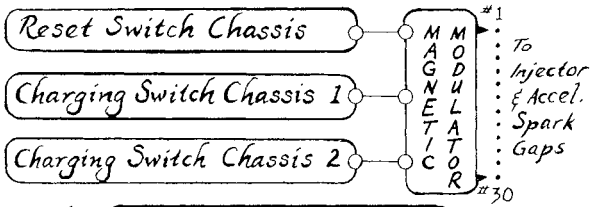

Fig 4b New Magnetic Trigger

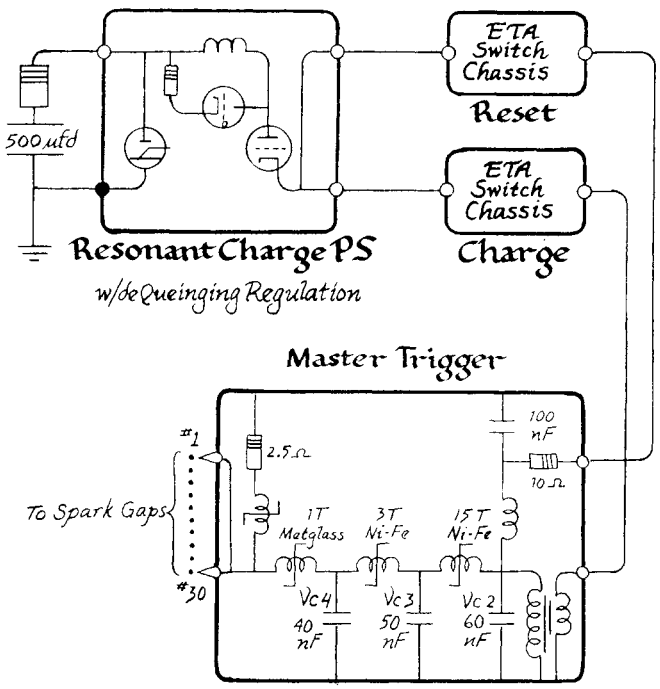

Fig 5 ETA Magnetic Trigger System

Fig 6 Waveforms

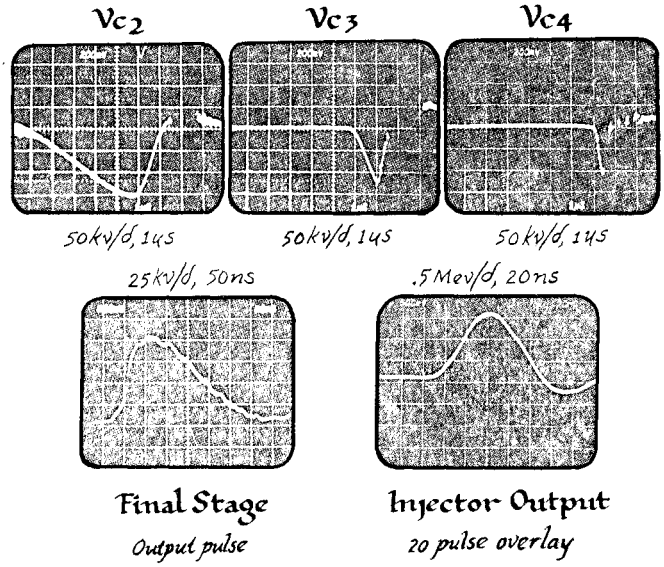

Summary and Conclusions

The magnetic pulse generators that were constructed and tested demonstrated that the theory certainly applies to high peak power levels (10^{10} watts). The circuits used were similar to those previously described and applied to radar pulse modulators. The availability of new magnetic materials (metglas) of better quality and thickness, allowed us to advance the state of the art at least an order of magnitude in pulse compression and risetime over previously described generators. There are many details and additional problems that have not been addressed here. Large output voltage variations are limited with a fully magnetic system. The Blumlein current with a fast charging pulse will cause ringing when the same current is used to reset the accelerator cell. Although jitter is directly attributed to input charging voltage amplitude and time variations, paralleling of many magnetic pulse generator should be investigated further. The characteristics of core materials for the critical final stage are certainly acceptable. The dynamic losses, including hysterisis and eddy currents were quite low. It would certainly be desirable to obtain cores which are insulated turn to turn and also magnetically annealed to achieve better performance.

In conclusion, it indeed appears possible to construct magnetic switches which are very competitive in cost with existing gas blown sparkgap systems with very similar output pulse characteristics. The primary advantages lie in their inherent reliability, high rep-rate and noiseless operation.

APPENDIX A:
Determination of μ_{sat} and μ_{unsat}

A. Determination of μ_{sat}

Low field measurements of many magnetic materials give the appearance of saturation at fields slightly above Hc. In fact μ_{sat} is never equal to μ_0, but will begin to approach μ_0 at the anisotropy field H_k. Some measurements on

Metglass 2826 conducted at Allied Chemical[3,4] (see Fig. A-1) illustrate this affect. Measurements on various other materials are depicted graphically in Fig. A-2.

When designing a magnetic amplifier, one must take this behavior into account in order to achieve satisfactory operation.

B. Determination of μ_{unsat}

Because of frequency-dependent losses, the saturation field H_{sat} is larger at high frequencies than is the dc value. Therefore, the high-frequency effective μ_{unsat} will be less than that indicated by low frequency measurements. The saturation magnetization B_s is relatively independent of frequency.

In the brief analysis which follows below we will try to generate an approximate relationship between μ_{unsat} and the energy loss in the core

$$\frac{\text{Energy loss}}{\text{Volume}} = \int_{B_r}^{B_s} H \cdot dB = \langle H \rangle \cdot B_s \quad ,$$

but $\Delta B_s \approx \bar{\mu}_{unsat} \cdot H_{sat}$; and if $\langle H \rangle \sim H_{sat}/2$ then

$$\frac{\text{Energy loss}}{\text{Volume}} \approx \frac{(\Delta B_s)^2}{2 \cdot \bar{\mu}_{unsat}} \quad ,$$

and

$$\bar{\mu}_{unsat} \approx \frac{(\Delta B_s)^2}{2 \cdot \left(\frac{\text{Energy lost}}{\text{Volume}}\right)} \quad .$$

APPENDIX B:
Calculation of Core Losses

There are three primary contributions to the core loss, the dc anisotropy energy, eddy current losses, and spin relaxation viscous damping. The dc anisotropy energy can be determined by measuring

$$\int_{B_r}^{B_s} B \cdot dH$$

at low frequencies, but the eddy current and spin relaxation losses vary with frequency.

The losses in the metallic-tape-wound cores is strongly influenced by the above frequency dependent effects. Examination of these cores indicates that a saturation wave begins at the surface of the tapes and propagates toward the center. The propagation velocity is simply the domain wall velocity[3] and is given by

$$v = \left(\frac{2 B_s}{\beta}\right)(H - H_0) \quad [\text{CGS}] \quad ,$$

where H_0 is the dc saturation field and is given by

$$\tilde{\beta} = \beta_e + \beta_r \quad ,$$

with β_e (β_r) being the eddy current (spin relaxation) viscous damping parameter. The saturation field of a tape of thickness d is approximately

$$H \approx H_0 \text{ dc} + \frac{d \cdot \beta}{4 B_s \tau_{sat}} \quad .$$

where

$$\beta_e = \frac{(16 \cdot B_s)^2 d}{\pi \cdot \rho \cdot c^2} \quad [\text{CGS}] \, ,$$

and

$$\beta_r = \left[\alpha(1 + \alpha^2) \; B_s/\gamma\right] \left(\frac{k}{A}\right)^{1/2} [\text{CGS}] \, ,$$

where γ is the gyromagentic ratio, k the anisotropy energy, α the Gilbert damping parameter, and A the exchange stiffness constant.

Calculations[5] concerning core losses are presented graphically in Fig. B-1 reference 3.

References

1. W.S. Melville, "The Use of Saturable Reactors as Discharge Devices for Pulse Generators," Proceedings Institute of Electrical Engineers, (London) Vol. 98, Part 3 (Radio and Communication), No. 53, 1951, p. 185.

2. R.A. Mathias and E.M. Williams, "Economic Design of Saturating Reactor Magnetic Pulsers," Transactions of the American Institute of Electrical Engineers, Vol. 74, Part I (1955).

3. D.L. Birx, "Basic Principles Governing the Design of Magnetic Switches", UCID 18831, Nov. 18, 1980.

4. M.F. Thompson, R.R. Trautwein, and E.R. Ingersoll, "Magnetic Pulse Generator Practical Design Limitations," Communication and Electronics, Number 28, January 1957, p. 789.

5. E.J. Smith, "Design and Performance of Pulse Magnetic Modulators," Proceedings of Fifth Symposium of Hydrogen Thyratrons and Modulators, May 1958, p. 112.

6. E.M. Lassiter, P.R. Johannessen, and R.H. Spencer, "High Power Pulse Generation Using Semiconductors and Magnetic Cores," Proceedings Special Technical Conference on Nonlinear Magnetics and Magnetic Amplifiers, September 1959, p. 215.

7. E.W. Manteuffel, and R.E. Cooper, "Direct Current Charged Magnetic Pulse Modulator," Proceedings Special Technical Conference on Nonlinear Magnetics and Magnetic Modulators, September 1959, p. 234.

8. E.M. Goldfard, "Performance of 9.6 MW Magnetic Pulse Modulator Prototype," Proceedings of the Sixth Symposium on Hydrogen Thyratrons and Modulators, May 1960, p. 235.

9. R. O'Handley, L.I. Mendelson, R. Hasegawa, R. Ray, and S. Kauesh, "Low-Field Magnetic Properties of $Fe_{80}B_{20}$ Glass," Journal of Applied Physics, Vol. 47, No. 10 (October 1976).

Acknowledgment

I would like to thank George Butner for his time spent in drawing the illustrations for this paper.

The Lawrence Livermore National Laboratory is operated by the University of California for the Department of energy under Contract No. W-7405-Eng-48.

This work is performed by LLNL for the Department of Defense under DARPA (DoD) ARPA Order 3718, Amendment #33 and 34, monitored by NSWC under Contract No. N60921-81-LT-W0009, Amendment 1 and N60921-81-LT-W0026.